# Supplement: Visual Analysis of Electronic Densities and Transitions in Molecules

T. Bin Masood [†] [1] , S.S. Thygesen [1] , M. Linares [1,2] , A. I. Abrikosov [1] , V. Natarajan [‡] [3] , and I. Hotz [1]

[1]Department of Science and Technology (ITN), Linköping University, Norrköping, Sweden
[2]Laboratory of Organic Electronics, Linköping University, Norrköping, Sweden
[3]Indian Institute of Science, Bangalore, India

## Abstract

*This document contains supplemental data and figures for the paper "Visual Analysis of Electronic Densities and Transitions in Molecules".*

## 1. Comparison of Voronoi segmentation with gradient-based segmentation

For segmenting charge density field spatially among the atoms of the molecule, gradient-based partitioning was suggested by Bader [Bad90]. In practice, this idea has been implemented in software like TopoMS [BGL*18] and an implementation by Henkelman *et al.* [HAJ06]. However, both these software failed to generate a segmentation for our input charge density fields *i.e.* NTOs. We believe this is because of the fact that these software are tailored for analysis of *full* charge density fields. The NTO charge density however is different, for example, it may not have any charge density maxima corresponding to some atoms, which is a crucial assumption made by both these software, resulting in failure to generate a segmentation.

In order to compare the Voronoi segmentation with some gradient-based approach, we then decided to use the Morse-Smale complex as implemented in Topology Toolkit (TTK) [TFL*17]. It uses discrete Morse theory for computation of combinatorial gradient-based segmentation. To compute the segmentation, as a first step the maxima along with their ascending manifolds are computed using TTK. The ascending manifold of a maximum is the set of all points in the domain which reach this maximum after repeated integration in the gradient direction. Then in the second step, we used an approach suggested by TopoMS to assign a maximum to the closest atom, to compute the segmentation and charge per atom. The atomic charge can then be added to compute the subgroup charges.

Table S1 lists this detailed comparison for all the data sets used in our case studies. We can observe that Voronoi and gradient-based techniques provide very similar division of charge at the level of subgroups. The instances where the charge computed by Voronoi and Morse complex based approaches differ by more than 2% are highlighted in red. We observed only 6 such cases out of 102 computations of charges at the level of subgroup. Five of these six cases are observed in the case of metal complexes where one of the subgroups consist of just atom which can result in more noticeable differences in atomic boundaries.

## References

[Bad90] BADER R. F. W.: *Atoms in molecules – A Quantum Theory*. International Series of Monographs on Chemistry. Wiley Online Library, 1990. 1

[BGL*18] BHATIA H., GYULASSY A. G., LORDI V., PASK J. E., PASCUCCI V., BREMER P.-T.: TopoMS: Comprehensive topological exploration for molecular and condensed-matter systems. *Journal of Computational Chemistry 39*, 16 (2018), 936–952. 1

[HAJ06] HENKELMAN G., ARNALDSSON A., JÓNSSON H.: A fast and robust algorithm for Bader decomposition of charge density. *Computational Materials Science 36*, 3 (2006), 354–360. 1

[TFL*17] TIERNY J., FAVELIER G., LEVINE J. A., GUEUNET C., MICHAUX M.: The topology toolkit. *IEEE Transactions on Visualization and Computer Graphics (TVCG) 24*, 1 (2017), 832–842. 1

[†] {talha.bin.masood | signe.sidwall.thygesen | mathieu.linares | alexei.abrikossov | ingrid.hotz}@liu.se
[‡] vijayn@iisc.ac.in

| | Molecule | State | Subgroup | $Q^h$ | | | $Q^p$ | | |
|---|---|---|---|---|---|---|---|---|---|
| | | | | $Q^h_{Vor}$ | $Q^h_{MC}$ | $\|Q^h_{Vor} - Q^h_{MC}\|$ | $Q^p_{Vor}$ | $Q^p_{MC}$ | $\|Q^p_{Vor} - Q^p_{MC}\|$ |
| Case study 1 | Thiophene-Quinoxaline | State 1 | THIO | 54.8% | 54.8% | **0.0%** | 6.8% | 5.8% | **1.0%** |
| | | | QUIN | 45.2% | 45.2% | **0.0%** | 93.2% | 94.2% | **1.0%** |
| | | State 4 | THIO | 94.2% | 94.4% | **0.2%** | 7.1% | 6.0% | **1.1%** |
| | | | QUIN | 5.8% | 5.6% | **0.2%** | 92.9% | 94.0% | **1.1%** |
| | | State 9 | THIO | 16.5% | 16.4% | **0.1%** | 2.1% | 1.8% | **0.3%** |
| | | | QUIN | 83.5% | 83.6% | **0.1%** | 97.9% | 98.2% | **0.3%** |
| Case study 2 | [6]cycloparaphenylene | State 1 | PHE1 | 13.2% | 13.2% | **0.0%** | 20.3% | 20.7% | **0.4%** |
| | | | PHE2 | 15.6% | 15.6% | **0.0%** | 17.6% | 17.6% | **0.0%** |
| | | | PHE3 | 19.2% | 19.2% | **0.0%** | 14.1% | 13.8% | **0.3%** |
| | | | PHE4 | 14.0% | 14.0% | **0.0%** | 19.2% | 19.3% | **0.1%** |
| | | | PHE5 | 20.4% | 20.4% | **0.0%** | 13.2% | 13.0% | **0.2%** |
| | | | PHE6 | 17.6% | 17.6% | **0.0%** | 15.6% | 15.6% | **0.0%** |
| | | State 2 | PHE1 | 0.7% | 0.5% | **0.2%** | 37.9% | 39.7% | **1.8%** |
| | | | PHE2 | 0.7% | 0.5% | **0.2%** | 38.0% | 39.4% | **1.4%** |
| | | | PHE3 | 11.4% | 11.4% | **0.0%** | 10.5% | 8.9% | **1.6%** |
| | | | PHE4 | 11.4% | 11.4% | **0.0%** | 10.5% | 9.2% | **1.3%** |
| | | | PHE5 | 37.9% | 38.0% | **0.1%** | 1.5% | 1.4% | **0.1%** |
| | | | PHE6 | 37.9% | 38.0% | **0.1%** | 1.5% | 1.4% | **0.1%** |
| | | State 3 | PHE1 | 3.3% | 3.2% | **0.1%** | 24.1% | 23.6% | **0.5%** |
| | | | PHE2 | 24.8% | 24.9% | **0.1%** | 3.1% | 2.6% | **0.5%** |
| | | | PHE3 | 43.3% | 43.4% | **0.1%** | 1.8% | 1.8% | **0.0%** |
| | | | PHE4 | 0.5% | 0.4% | **0.1%** | 43.8% | 46.1% | **<span style="color:red">2.3%</span>** |
| | | | PHE5 | 24.8% | 24.9% | **0.1%** | 3.1% | 2.6% | **0.5%** |
| | | | PHE6 | 3.3% | 3.2% | **0.1%** | 24.1% | 23.3% | **0.8%** |
| Case study 3 | Cu-PHE2 | State 1 | Cu | 71.6% | 70.3% | **1.3%** | 3.5% | 1.8% | **1.7%** |
| | | | PHE1 | 13.8% | 14.3% | **0.5%** | 42.7% | 43.4% | **0.7%** |
| | | | PHE2 | 14.6% | 15.4% | **0.8%** | 53.8% | 54.8% | **1.0%** |
| | Ag-PHE2 | State 1 | Ag | 52.3% | 49.8% | **<span style="color:red">2.5%</span>** | 2.7% | 0.7% | **2.0%** |
| | | | PHE1 | 23.0% | 24.3% | **1.3%** | 46.8% | 47.8% | **1.0%** |
| | | | PHE2 | 24.7% | 25.9% | **1.2%** | 50.5% | 51.5% | **1.0%** |
| | Au-PHE2 | State 1 | Au | 50.2% | 49.1% | **1.1%** | 2.8% | 1.3% | **1.5%** |
| | | | PHE1 | 29.8% | 30.4% | **0.6%** | 46.9% | 47.6% | **0.7%** |
| | | | PHE2 | 20.0% | 20.6% | **0.6%** | 50.3% | 51.1% | **0.8%** |
| Case study 4 | Cu-PHE2 | State 1 | Cu | 71.6% | 70.3% | **1.3%** | 3.5% | 1.8% | **1.7%** |
| | | | PHE1 | 13.8% | 14.3% | **0.5%** | 42.7% | 43.4% | **0.7%** |
| | | | PHE2 | 14.6% | 15.4% | **0.8%** | 53.8% | 54.8% | **1.0%** |
| | Cu-PHE-PHEPHE | State 1 | Cu | 67.9% | 66.5% | **1.4%** | 3.2% | 1.7% | **1.5%** |
| | | | PHE | 12.9% | 13.7% | **0.8%** | 59.2% | 60.5% | **1.3%** |
| | | | PHEPHE | 19.2% | 19.8% | **0.6%** | 37.6% | 37.8% | **0.2%** |
| | Cu-PHE-PHEME | State 1 | Cu | 70.9% | 69.9% | **1.0%** | 3.6% | 2.0% | **1.6%** |
| | | | PHE | 16.9% | 18.0% | **1.1%** | 95.7% | 97.3% | **1.6%** |
| | | | PHEME | 12.2% | 12.1% | **0.1%** | 0.7% | 0.6% | **0.1%** |
| | Cu-PHE-PHEOME | State 1 | Cu | 66.5% | 65.8% | **0.7%** | 3.2% | 1.9% | **1.3%** |
| | | | PHE | 14.7% | 15.5% | **0.8%** | 95.8% | 97.4% | **1.6%** |
| | | | PHEOME | 18.8% | 18.7% | **0.1%** | 1.1% | 0.7% | **0.4%** |
| | Cu-PHE-IPR | State 1 | Cu | 71.4% | 70.8% | **0.6%** | 4.1% | 1.5% | **<span style="color:red">2.6%</span>** |
| | | | PHE | 23.0% | 24.9% | **1.9%** | 93.8% | 97.2% | **<span style="color:red">3.4%</span>** |
| | | | IPR | 5.6% | 4.3% | **1.3%** | 2.0% | 1.3% | **0.7%** |
| | Cu-PHE-XANT | State 1 | Cu | 35.1% | 30.6% | **<span style="color:red">4.5%</span>** | 2.3% | 1.2% | **1.1%** |
| | | | PHE | 8.0% | 7.9% | **0.1%** | 95.5% | 97.1% | **1.6%** |
| | | | XANT | 56.9% | 61.5% | **<span style="color:red">4.6%</span>** | 2.2% | 1.7% | **0.5%** |

**Table S1:** *Comparison of subgroup charges computed using the Voronoi-based approach and the Morse complex-based approach. The symbols $Q^h_{Vor}$ and $Q^h_{MC}$ are used to denote the subgroup charge for hole NTO computed using Voronoi diagram-based and Morse complex-based approaches. Similarly, $Q^p_{Vor}$ and $Q^p_{MC}$ are used for particle NTO charges. The entries where the two approaches differ by more than 2% are highlighted in red.*
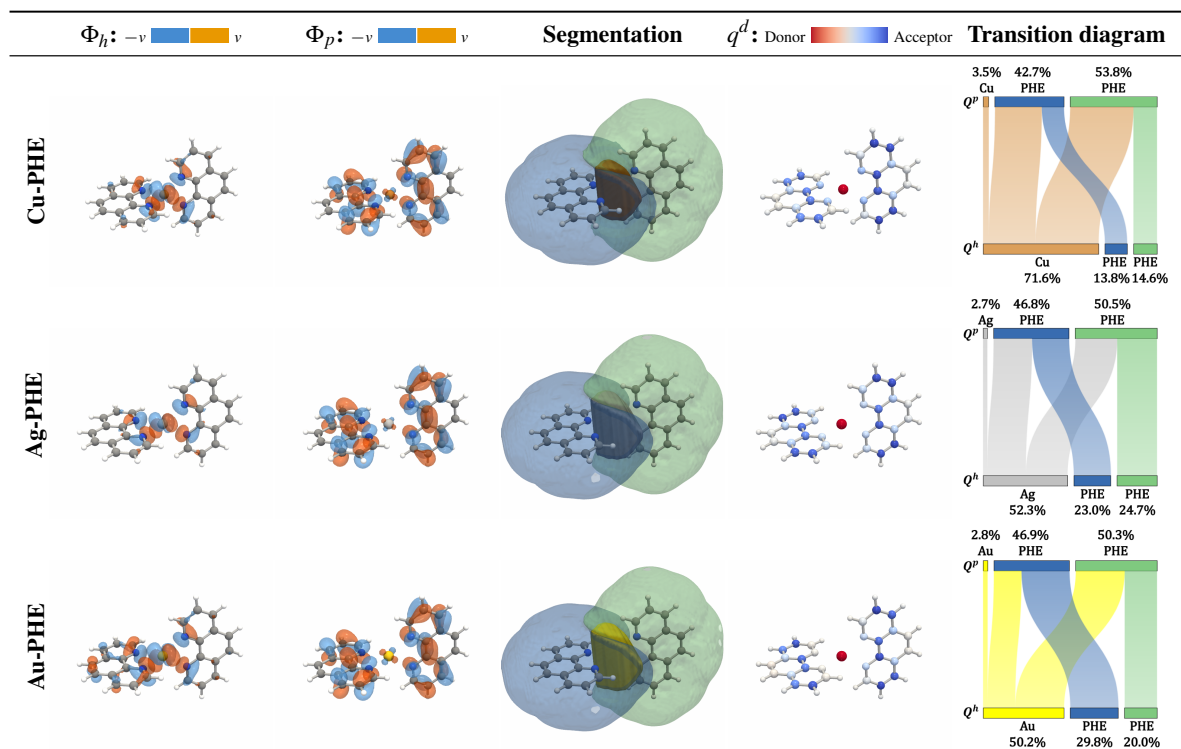
**Figure S1:** *Case study 3: Metal complexes (Section 6.3). Cols. 1 and 2 relate to visualization task V1. They show the isosurfaces for the different NTOs for the hole (col. 1) and particle (col. 2). Col. 3 shows the segmentation of the different subgroups. Col. 4 shows the results of V2, displaying how the charge changes during the electronic excitation at atomic level of detail. Col. 5 displays the results of V3, showing the transition diagram for the different metal complexes.*
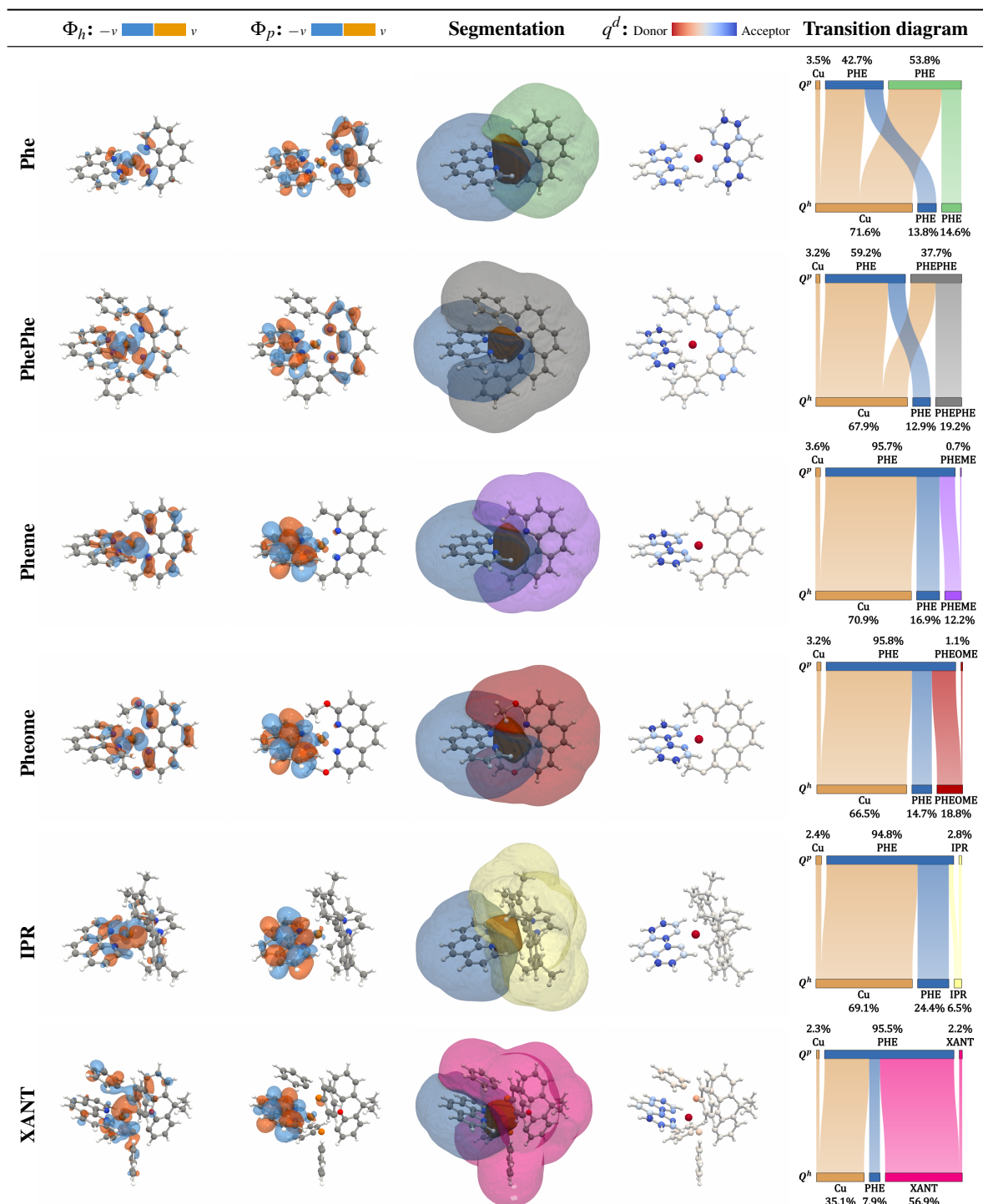
**Figure S2:** *Case study 4: Copper complexes with various ligands (Section 6.4). Columns 1 and 2 show selected isosurfaces for the hole and particle NTOs respectively. Column 3 shows the volume segmentation for the different subgroups. Column 4 shows how the charge changes during the electronic excitation. The last column shows the transition diagram for the different ligands. Notice how the transition diagrams in top two rows (*Phe *and* PhePhe*) are similar and how they differ from the second category, the next four rows.*